High-numerical-aperture-based virtual point detectors for photoacoustic tomography

Changhui Li[a)] and Lihong V. Wang[b)]

Optical Imaging Laboratory, Department of Biomedical Engineering Washington University in St.Louis, St.Louis, Missouri 63130, USA

The focal point of a high-numerical-aperture (NA) ultrasonic transducer can be used as a virtual point detector. This virtual point detector detects omnidirectionally over a wide acceptance angle. It also combines a large active transducer surface and a small effective virtual detector size. Thus the sensitivity is high compared with that of a real point detector, and the aperture effect is small compared with that of a finite size transducer. We present two kinds of high-NA-based virtual point detectors and their successful application in photoacoustic tomography. They can also be applied in other ultrasound-related fields. © *2008 American Institute of Physics*. [DOI: 10.1063/1.2963365]

Photoacoustic (PA) tomography (PAT) is a promising nonionizing, noninvasive biomedical imaging modality.[1,2] It combines sensitive optical contrast and high ultrasonic resolution and has been successfully applied in imaging both small animal and human tissues.[3–5] However, the ultrasonic transducer's finite aperture limits the image resolution[6] and, due to its limited acceptance angle, also limits the field of view of the detection system. In practice, pointlike ultrasonic detectors have never been used in PAT because of its poor sensitivity, caused by their high thermal noise level.

Previously, a ring-based virtual point detector was introduced for PAT,[7] which works like an ideal point detector with high sensitivity. However, the ring-based virtual point detector has a limited imaging region, and it also requires that the object be smaller than the ring. Another virtual point detector method, using a positively focused ultrasonic transducer, was previously introduced in Ref. 8 for photoacoustic microscopy (PAM), and its possible application in PAT was also numerically studied.[9] In this letter, we extend the second method to include negatively focused transducers, and we are able to construct NA=1 transducers to demonstrate their power to be used as virtual point detectors.

The radiation pattern of a focused transducer, at a certain frequency f, is shown in Fig. 1. If the transducer's active surface is part of a spherical shell with a radius of R, the focal point F is at the sphere's center. Owing to diffraction, emitted ultrasound waves are not focused to an infinitesimal point at F; however, they are focused to a small region with a finite beam diameter (BD). From there, the waves diverge into a region limited by the beam spread angle θ_b. From the principle of reciprocity, the radiation pattern also describes the detection pattern.

The BD describes how narrowly the ultrasound can be focused at the focal point, and it is determined by the numerical aperture (NA) and wavelength. In this letter, we use the full width at half maximum of the field magnitude, where the field magnitude at the beam boundary is half of that at the focal point, to determine the BD. When the wavelength is much less than the size of the transducer, the amplitude of the emitted field at location P in Fig. 2(a), Δl away from the focal point F, can be approximately calculated by the Rayleigh integral as[10]

$$A(\Delta l) \propto \int_0^{\theta_{\max}} \int_0^{2\pi} e^{ik\Delta l \sin(\theta)\cos(\phi)} \sin(\theta) d\theta d\phi$$

$$= \int_0^{\theta_{\max}} J_0[k\Delta l \sin(\theta)]\sin(\theta)d\theta, \tag{1}$$

where θ and ϕ are the polar and azimuthal angles, respectively, J_0 is the Bessel function of the first kind, $k=2\pi/\lambda$, and λ is the wavelength. By numerically solving the solution of $A(\Delta l)=A(0)/2$ ("$|\cdots|$" represents an absolute value), we obtained the relation between BD and NA, as seen in Fig. 2(b). This relation can be approximately fitted by the function

$$\text{BD} \approx 0.62 \frac{\lambda}{\text{NA}}. \tag{2}$$

Equation (2) tells us that the BD decreases as the transducer's NA increases. To achieve a "pointlike" virtual detector by using the focal point of a positively focused transducer, high-NA transducers are required. In addition, by using a high-NA transducer, the effective size of the virtual point detector is less than the wavelength, leading to a wide omnidirectional detection angle θ_b over a broad bandwidth.
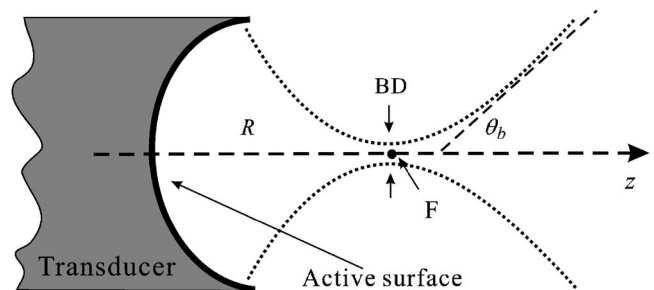

FIG. 1. The radiation pattern of a positively focused ultrasonic transducer. The transducer has a spherical curved surface with a radius of R, and the focal point F lies at the center of the sphere. The emitted ultrasound is focused to a region with a finite BD. After passing the focal zone, the radiation diverges into a region limited by the beam spread angle θ_b.

a)Electronic mail: cli@biomed.wustl.edu.
b)Author to whom correspondence should be addressed. Electronic mail: lhwang@biomed.wustl.edu.

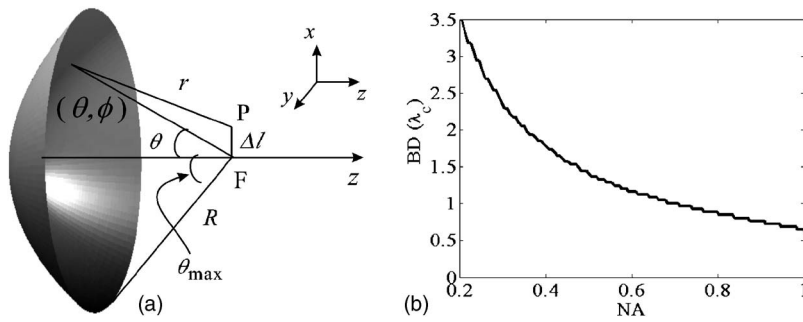**93**, 033902-1

FIG. 2. (a) The spherical shell represents the transducer's surface; z-axis is the transducer's symmetry axis; θ and ϕ are the polar and azimuthal angles; F is the focal point, and P is an arbitrary nearby point, Δl away from F; θ_{max} is the maximum polar angle, hus NA $= \sin(\theta_{max})$. (b) BD vs NA. The BD is normalized by the wavelength λ.

Similarly, a negatively focused ultrasonic transducer can also be used as a virtual point detector. It differs from a positively focused transducer in that the virtual point detector is located behind the real detection surface. Figure 3(a) represents a virtual point detector by using a negatively focused transducer, and Fig. 3(b) is a positively focused counterpart.

The image reconstruction method used with the virtual point detector is almost the same as the one used with real point detectors, except for minor modifications in the signal time delay, which is due to the spatial difference between the locations of the virtual point detector and the transducer's active surface. The modifications are, respectively,

- $t = t_d + R/c$ for a negative focused virtual point detector and
- $t = t_d - R/c$ for a positive focused virtual point detector,

where t is the time delay used in image reconstructions, t_d is the real detection time, R is the radius of the positively or negatively focused ultrasonic transducer, and c is the acoustic speed.

A metallized polyvinylidene fluoride (PVDF) film (from Measurement Specialties, Inc.), with a thickness of 110 μm, was used to construct the transducer. Because the flat PVDF film was not suitable to be stretched into a spherical shell, we constructed two dimensional (2D) transducers by bending strips of the film into the half circular shapes seen in Fig. 3. These 2D transducers have NA=1. The PVDF films of the negatively focused and positively focused transducers were all 6.0 mm in width, and their radii were 12 and 13 mm, respectively. The PVDF films were glued to acrylic plastic surfaces, and the estimated center frequency was around 6.0 MHz. To compare with flat transducers, we further constructed a square flat PVDF transducer (5.0×5.0 mm^2).

According to this construction and the center frequency, the Rayleigh integral was used to calculate the focal width,[10] i.e., the effective virtual point detector size, to be around 120 μm, about half of the wavelength of the center frequency. This subwavelength virtual detector also has a very

broad uniform acceptance angle (close to $\pi/2$), which is another key characteristic of ideal point detectors.

Tissue phantoms were imaged by these virtual point detectors in PAT. As shown in Fig. 4, the PA source contained three black human hair crosses glued on top of optical fibers, with an interval between the hair samples of about 1.0 cm. A neodymium doped yttrium aluminum garnet laser (Brilliant B, Quantel) generated 6.5 ns, 532 nm laser pulses with a repetition rate of 10 Hz, which were diverged by a ground glass, so that all three hair crosses were illuminated. Both the phantom and the transducer were immersed in a tank filled with water. The virtual point detectors evenly scanned the object along a horizontal circle, stopping at 240 points, and the signals were averaged at 20 times at each stop. The PA signals were first amplified at 40 dB by a preamplifier, and then were recorded by an oscilloscope (Tektronix TDS640A) with a sampling rate of 50 MHz. Finally, the recorded signals were sent to a PC for image reconstruction.

The hair phantoms were scanned by the two virtual point detectors and a flat transducer. Figure 5(a) shows the result of scanning with a positively focused transducer; the scanning radius relative to its focal point was about 2.3 cm. Figure 5(b) shows the result of scanning with a negatively focused transducer; the scanning radius relative to its focal point was about 4.2 cm. Figure 5(c) shows the result of scanning with a flat transducer; the scanning radius was about 3.0 cm.

Although these three experiments had comparably short scanning distances, the results were clearly different. Both images in Figs. 5(a) and 5(b), which were reconstructed from data obtained by two virtual point detectors, presented complete reconstructions with a high and uniform signal-to-noise-ratio (SNR). However in Fig. 5(c), owing to the aperture effect and the limited acceptance angle, the image not only was blurred at the ends of each hair but also almost completely failed to detect the horizontal hairs on the left and right phantoms.

To alleviate the image blurring and incompleteness, the finite size flat transducer had to be put much further away
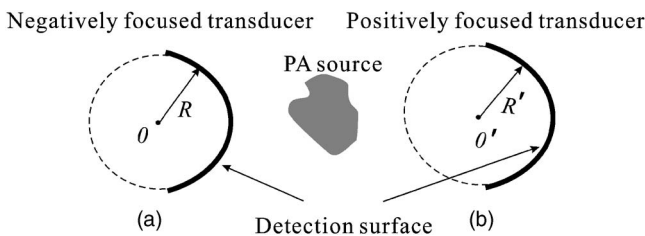
FIG. 3. Two kinds of virtual point detectors. (a) The negatively focused transducer; the virtual point is located behind the detection surface. (b) The positively focused transducer; the virtual point is located in front of the detection surface.
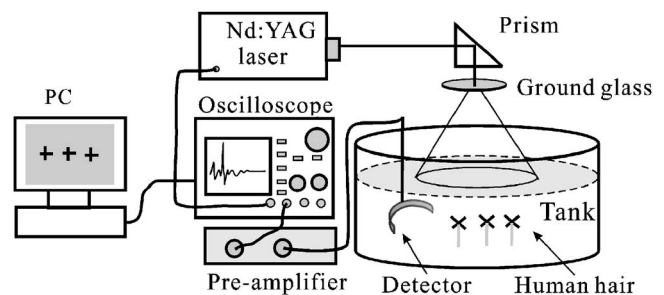
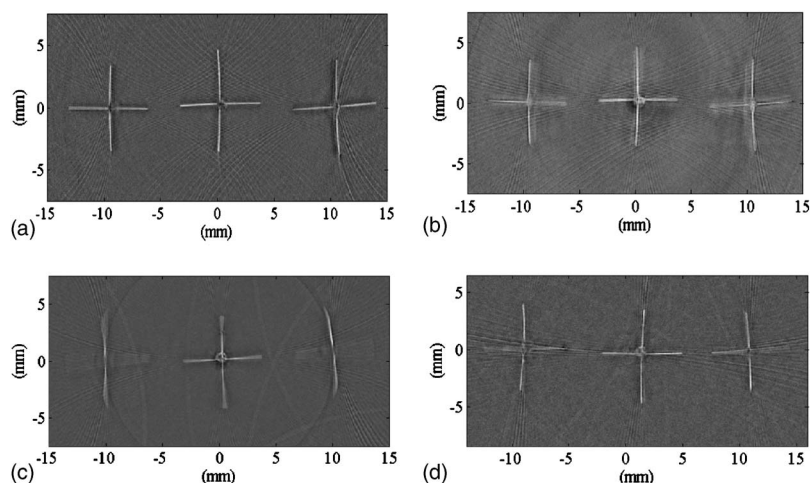FIG. 4. Experimental setup of the phantom experiments.

FIG. 5. Reconstructed PAT images. (a) From data gathered by a positively focused PVDF transducer, the scanning radius of the virtual point was 2.3 cm. (b) From data gathered by a negatively focused PVDF transducer, the scanning radius of the virtual point was 4.2 cm. (c) From data gathered by a flat transducer, the scanning radius was 3.3 cm. (d) From data gathered by a flat transducer, the scanning radius was 8.8 cm.

from the scanning center, at the expense of signal strength. Figure 5(d) shows the result for the flat transducer at 8.8 cm from the center, a distance that yielded a lower SNR than in Fig. 5(c). Even at this long scanning distance, the images of the left and right horizontal hairs were still partially blurred in comparison with Figs. 5(a) and 5(b). Thus, this phantom experiment demonstrated the advantages of the virtual point detectors over the flat transducer.

In summary, both theoretical analysis and phantom experiments demonstrate that high-NA-based virtual point detectors offer significant improvements over a flat transducer in PAT. Without losing sensitivity relative to flat transducers, virtual point detectors have a negligible aperture effect and a wide acceptance angle, so they can be put close to the PA source, where the signals are strong, maximizing the SNR. Compared with the ring-based virtual point detector,[7] the high-NA-based virtual point detector can also be used like any other kind of single ultrasonic transducer to image arbitrarily sized and shaped objects. Moreover, they can also be used to build an ultrasonic transducer array. In addition to PAT, this idea can also be used in microwave-induced thermoacoustic tomography, where the laser is replaced with a microwave source. These virtual point detectors can also be implemented in other tomography methods or technologies that use ultrasonic detectors, such as ultrasonic tomography.

[1] M. H. Xu and L. H. V. Wang, Rev. Sci. Instrum. **77**, 041101 (2006).
[2] L. V. Wang and H.-i. Wu, *Biomedical Optics: Principles and Imaging* (Wiley, Hoboken, NJ, 2007).
[3] C. G. A. Hoelen, F. F. M. de Mul, R. Pongers, and A. Dekker, Opt. Lett. **23**, 648 (1998).
[4] X. D. Wang, Y. J. Pang, G. Ku, X. Y. Xie, G. Stoica, and L. H. V. Wang, Nat. Biotechnol. **21**, 803 (2003).
[5] R. I. Siphanto, K. K. Thumma, R. G. M. Kolkman, T. G. van Leeuwen, F. F. M. de Mul, J. W. van Neck, L. N. A. van Adrichem, and W. Steenbergen, Opt. Express **13**, 89 (2005).
[6] M. Xu and L. V. Wang, Phys. Rev. E **67**, 056605 (2003).
[7] X. M. Yang, M. L. Li, and L. H. V. Wang, Appl. Phys. Lett. **90**, 251103 (2007).
[8] M. L. Li, H. F. Zhang, K. Maslov, G. Stoica, and L. H. V. Wang, Opt. Lett. **31**, 474 (2006).
[9] M. L. Li and L. H. V. Wang, in *SPIE International Symposium on Biomedical Optics* (SPIE, San Jose, CA, 2007), Vol. 6437.
[10] A. D. Pierce, *Acoustics: An Introduction to Its Physical Principles and Applications* (Acoustical Society of America, New York, 1989).